Calculations of effect of anisotropic stress/strain on dopant diffusion in silicon under equilibrium and nonequilibrium conditions

Scott T. Dunham[a)]
Department of Electrical Engineering, University of Washington, Seattle, Washington 98195

Milan Diebel and Chihak Ahn
Department of Physics, University of Washington, Seattle, Washington 98195

Chen Luen Shih
Department of Materials Science and Engineering, University of Washington, Seattle, Washington 98195

(Received 15 August 2005; accepted 21 November 2005; published 27 January 2006)

Understanding changes in dopant diffusion under strain is critical for controlling junction profiles in current and future very large scale integrated technology due to expanding use of large strains to enhance channel mobility. We use density functional theory calculations to investigate the stress dependence of boron (B) and arsenic (As) diffusion including vacancy (V) and interstitial (I) mechanisms under arbitrary stress/strain states. We have also analyzed the effects of stress on I and V diffusion with resulting impact on transient enhanced diffusion and coupled diffusion. For B diffusion, which is primarily mediated by I, we find greatly enhanced diffusion under tensile stress. Due to low symmetry of calculated transition state, we predict strongly anisotropic diffusion under anisotropic strain, with the strongest effects in direction of strain. This has a major impact on control of lateral junction abruptness as seen in two-dimensional simulations. The predicted behavior is consistent with combined analysis of vertical diffusion under biaxial [P. Kuo, J. L. Hoyt, J. F. Gibbons, J. E. Turner, and D. Lefforge, Appl. Phys. Lett. **66**, 580 (1995)] and hydrostatic [Zhao *et al.*] stress. In contrast, we find isotropic As diffusion for both I and V mediated processes. We predict As diffusivity to increase substantially under compressive strain, but to show little change under tensile strain, consistent with experimental observations [N. Sugii, J. Appl. Phys. **96**, 261 (2004)]. © *2006 American Vacuum Society.* [DOI: 10.1116/1.2151908]

I. INTRODUCTION

As ultralarge scale devices enter the nanoscale, stress effects become more important as steep doping gradients and heterointerfaces induce stress gradients and reduced dimensions make any variation in diffusivity critical. On top of this, stress is induced purposefully to enhance carrier mobility.[1–3] Since experiments are difficult and in the case of boron diffusion lead to contradictory results,[4] we utilize *ab initio* calculations to predict stress effects on the formation and migration of point defects and dopants. In contrast to previous work, our analysis extends beyond simple hydrostatic activation volumes[5] in order to be able to predict anisotropies associated with more complex stress states (e.g., differences between in-plane and perpendicular diffusion due to biaxial strain). We determine both strain tensors as well as changes in elastic constants due to defects and migration saddle points. In particular, earlier work on stress effects on I and V migration[6] is extended to determine stress effects on B and As diffusivities. Furthermore the results for I and B are combined using a simple transient enhanced diffusion (TED) model to estimate the effect of stress on boron diffusion during TED. Calculations are based on total energy of 64 atom supercells using the density functional theory (DFT) code VASP[7,8] in general gradient approximation with ultrasoft Vanderbilt pseudopotentials[9] and 2^3 Monkhorst–Pack k-point sampling.[10] B calculations were done with a 340 eV energy cutoff, with 250 eV cutoff for As. Transition states were obtained using nudged elastic band (NEB[11–13]) and climbing image[14] was used to get the energies of transition states.

II. BORON

B diffusion is dominated by the migration of an uncharged BI pair. Windl *et al.*[15] found the lowest migration

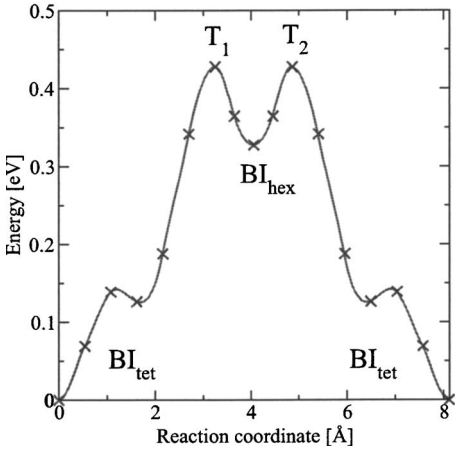

FIG. 1. B$I_{\text{tet}} \rightarrow$ B$I_{\text{hex}} \rightarrow$ BI_{tet} transition calculated using the NEB method (see Refs. 11–14) in unstrained Si (GGA Si equilibrium lattice parameter of 5.458 Å).

a)Author to whom correspondence should be addressed; electronic mail: dunham@ee.washington.edu

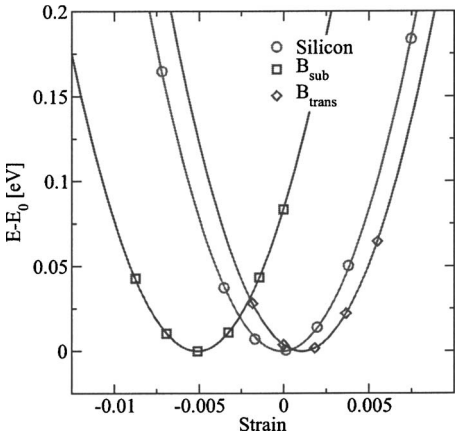

FIG. 2. Energy vs hydrostatic strain for Si, substitutional B, and BI transition state (B_{trans}) under hydrostatic strain. Strains are reported in reference to the GGA Si equilibrium lattice parameter. Energies are plotted relative to the minimum energy for given configuration, E_0.

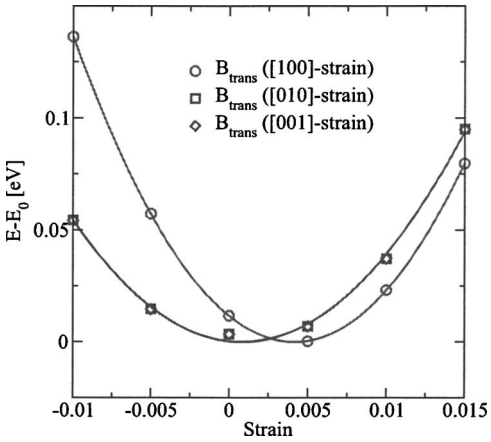

FIG. 4. Energy vs uniaxial strain in different directions for the transition state of $BI_{tet} \rightarrow BI_{hex}$ with hop vector $(3,1,1)b/8$, where b is the Si lattice constant. Note that the strain effect is largest in the dominant direction of motion.

barrier for uncharged BI to be $B_s + I^{tet} \rightarrow B_i^{hex} \rightarrow B_s + I^{tet}$, where B_i^{hex} is an interstitial B atom in a hexagonal site. In the following, $B_s + I^{tet}$ is written as BI^{tet}. Figure 1 shows the migration path for this transition in unstrained Si calculated using the NEB method. B diffusion, like that of self-interstitials,[6] involves a two-step process, with B_i^{hex} as the intermediate state. Both transitions result in displacement along ⟨311⟩ directions. To determine the effect of arbitrary stress on B diffusion, the induced strain $\Delta\boldsymbol{\epsilon}^{B_{trans}}$ (the deviation of the equilibrium lattice constant in the presence of the defect from that of pure Si) and modified elastic tensor $\Delta\mathbf{C}^{B_{trans}}$ of the transition state B_{trans} (T_1 or T_2 in Fig. 1) need to be determined.[6]

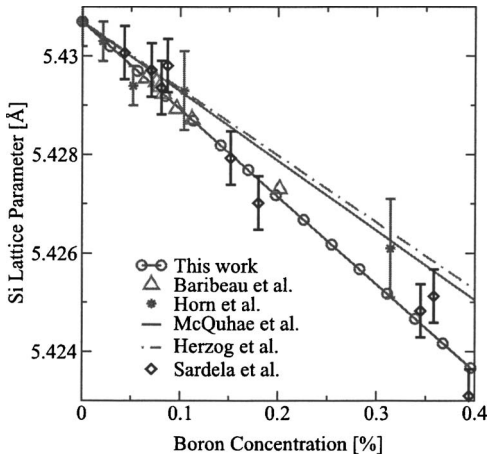

FIG. 3. Comparison of experimental data (see Ref. 26) with our *ab initio* results for the Si lattice parameter as a function of B concentration. The Si lattice constant can be expressed in terms of the induced strain $\Delta\epsilon$ of substitutional B and the fractional B concentration $x = C_B/C_S$ as $b = (1 + x\Delta\epsilon)b_{Si}$, where a_{Si} is the lattice parameter of bulk Si. $\Delta\epsilon = -0.327$ corresponds to a lattice contraction coefficient $\beta = 6.54 \times 10^{-24}$ cm^3. Sardela *et al.* report $\beta = (6.3 \pm 0.1) \times 10^{-24}$ cm^3 based on active B concentration. For other experiments, cluster formation at high B concentration may lead to lower strain levels.

The formation energy of the transition state is defined as: $E_f^{B_{trans}} = E_{B_{trans}} - E_{B_s} - E_{Si}/64$, where $E_{B_{trans}}$, E_{B_s}, and E_{Si} are the total energies of supercells containing B_{trans}, substitutional B (B_s), and defect-free Si, respectively. To determine the change in diffusivity, we only need to consider the variation of the formation energy of B_{trans} with respect to unstrained Si, $\Delta E_f^{B_{trans}}(\boldsymbol{\epsilon}) = E_f^{B_{trans}}(\boldsymbol{\epsilon}) - E_f^{B_{trans}}(0)$. Following the analysis in Ref. 6

$$\Delta E_f^{B_{trans}}(\boldsymbol{\epsilon}) = -\Omega_0(\Delta\boldsymbol{\epsilon}^{B_{trans}} - \Delta\boldsymbol{\epsilon}^{B_s}) \cdot \mathbf{C}^{Si} \cdot \boldsymbol{\epsilon} + \frac{\Omega_0}{2}\boldsymbol{\epsilon} \cdot (\Delta\mathbf{C}^{B_{trans}} - \Delta\mathbf{C}^{B_s} - \mathbf{C}^{Si}) \cdot \boldsymbol{\epsilon}, \quad (1)$$

where Ω_0 is volume per lattice site. This indicates that besides determining the elastic properties of B_{trans}, the induced strain and modified elasticity tensor of substitutional B ($\mathbf{C}^{B_s}$) also need to be calculated.

Figure 2 shows the energy dependence as a function of hydrostatic strain of a system with B_{trans}, B_s, and perfect Si. B_s exhibits a large negative induced strain, whereas B_{trans} shows a moderate positive induced strain. Due to the high symmetry of B_s, $\Delta\epsilon_x = \Delta\epsilon_y = \Delta\epsilon_z$.[6] The induced strain calculation has been compared to x-ray diffraction data and shows excellent agreement with the experimental observations (Fig. 3). Since B_{trans} does not have the high symmetry of B_s, additional energy versus strain relations were calculated to determine the induced strain vector $\Delta\boldsymbol{\epsilon}^{B_{trans}}$. Figure 4 shows the results for different uniaxial strain. B_{trans} shows different in-

TABLE I. Induced strains for B_s and B transition state extracted from Figs. 2 and 4.

		$\Delta\epsilon_\alpha$
B_s	$\Delta\epsilon_x = \Delta\epsilon_y = \Delta\epsilon_z$	−0.327
B_{trans}	$\Delta\epsilon_x$	+0.288
	$\Delta\epsilon_y$	−0.036
	$\Delta\epsilon_z$	−0.036

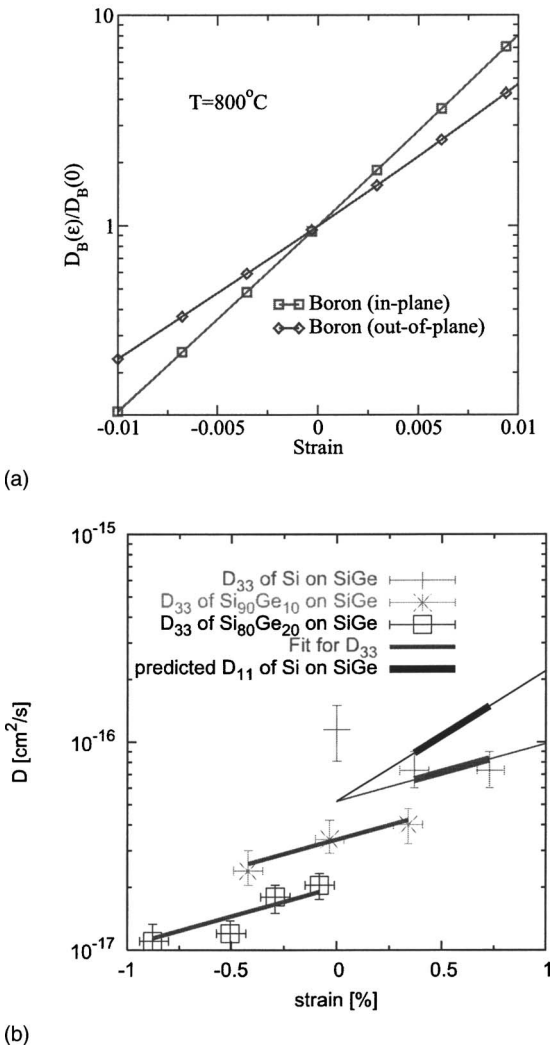

FIG. 5. B diffusion enhancement as a function of biaxial strain at 800 °C from (a) predictions based on DFT calculations, and (b) experimental data by Kuo *et al.* (see Ref. 16). The vertical B diffusion enhancement was measured under biaxial strain using SiGe bilayers with different Ge content (blue lines fitting data). The data were combined with hydrostatic B diffusion data from Aziz *et al.* (see Ref. 17) to estimate the lateral B diffusion enhancement (upper black line).

duced strains in the x direction (dominant direction of motion) in comparison to the y and z directions (which have identical induced strains). This is a clear indication of anisotropic B diffusion. Table I lists the induced strains for B_s and B_{trans} which were determined by fitting to the equation of state (see Ref. 6).

Based on the induced strains for B_s and B_{trans}, Fig. 5(a) shows the change in B diffusivity as a function of biaxial strain. The graph shows anisotropic behavior between in-plane (lateral) and out-of-plane (vertical) diffusion. The off-diagonal elements of the B diffusion tensor vanish. The predictions in Fig. 5(a) for vertical diffusion enhancement under biaxial strain can be compared to experimental data by Kuo *et al.*[16] shown in Fig. 5(b). Experimentally, the B diffusivity was determined in epitaxially grown SiGe bilayers with different Ge content to create a well defined biaxial strain state.

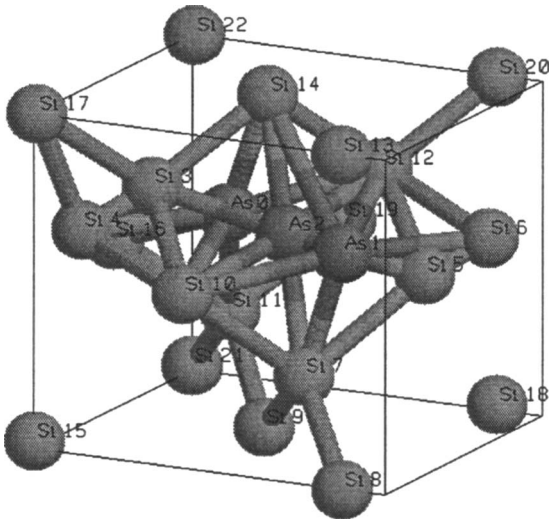

FIG. 6. Three-dimensional view of AsI migration. As$I_{\langle 110\rangle \text{split}} \rightarrow$ As$I_{\text{hex}} \rightarrow$ As$I_{\langle 110\rangle \text{split}}$. As migrates from a split position (As0 site) to another split position (As1 site) via hex site (As2 site). Si4 and As0 make $\langle 110\rangle$ split for Si lattice site of Si3. Si6 and As1 also make split for Si5. As As migrates from As0 to As1 position, the Si atom at Si4 site moves to original lattice point at Si3 site and Si atom at Si5 moves to Si6.

In the experiment, only the out-of-plane (vertical) B diffusivity was measured (blue lines). The B diffusivity enhancement was determined at different Ge concentrations and showed similar strain dependence. Combining these measurements with hydrostatic strain data by Aziz *et al.*[17] enables the determination of the in-plane (lateral) B diffusivity (black line) based on the relations between the hydrostatic and biaxial

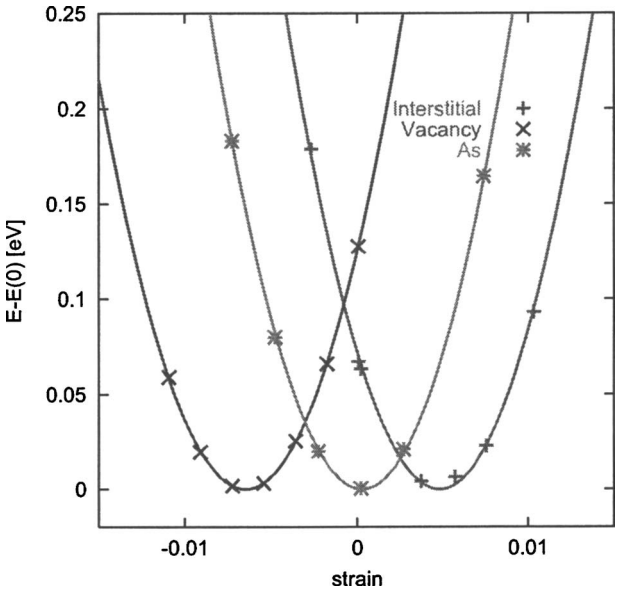

FIG. 7. Strain dependence of free energy for As complexes in 64 atom supercell. The magnitude of induced strain for As vacancy pair is slightly larger than that for transition state of As interstitial pair. Therefore the diffusivity enhancement/retardation is larger in vacancy mechanism. Energies are reported in reference to the minimum energy of each structure (energy in fully relaxed lattice). Strains are reported in reference to the GGA Si equilibrium lattice parameter.

TABLE II. Formation energies for various interstitial configurations. The ⟨110⟩ split has the lowest formation energy. The transition state of As*I* at hex site has a 0.5 eV higher energy than ⟨110⟩ split.

	⟨110⟩ split	⟨100⟩ split	Tet	Hex
E_f (eV)	3.1	4.0	4.3	3.6

activation volumes (see Refs. 5 and 18). Comparing the theoretical predictions shown in Fig. 5 with the experimental data shows general good agreement, however calculations predict a slightly stronger effect for both vertical and lateral B diffusion enhancement. Since there is still debate about the quality of the experimental measurements,[16,19] further measurements are necessary to confirm the experimental values.

III. ARSENIC

It is believed that As can diffuse via both interstitial and vacancy mechanisms.[20] The total diffusivity of isolated As in silicon is

$$D_{\mathrm{As}}^{\mathrm{total}}(\boldsymbol{\epsilon}) = D_{\mathrm{As}}^{I}(\boldsymbol{\epsilon}) + D_{\mathrm{As}}^{V}(\boldsymbol{\epsilon}) = D_{\mathrm{As}}^{I}(0)\exp\left(\frac{-\Delta E_f^{\mathrm{As}I_{\mathrm{trans}}}(\boldsymbol{\epsilon})}{kT}\right) + D_{\mathrm{As}}^{V}(0)\exp\left(\frac{-\Delta E_f^{\mathrm{As}V_{\mathrm{trans}}}(\boldsymbol{\epsilon})}{kT}\right), \quad (2)$$

where $D_{\mathrm{As}}^{I}(\boldsymbol{\epsilon})$ and $D_{\mathrm{As}}^{V}(\boldsymbol{\epsilon})$ are As diffusivity by interstitial and vacancy mechanisms, respectively, and $\Delta E_f^{\mathrm{AsI_{trans}}}$ and $\Delta E_f^{\mathrm{AsV_{trans}}}$ (equal for all transition states due to symmetry as discussed below) are changes in formation energies of transition states due to strain. The fractional interstitial contribution $f_I = D_{\mathrm{As}}^{I}/D^{\mathrm{total}}$ is given as

$$f_I(\boldsymbol{\epsilon}) = \frac{f_I(0)\exp\left(\frac{-\Delta E_f^{\mathrm{As}I_{\mathrm{trans}}}(\boldsymbol{\epsilon})}{kT}\right)}{f_I(0)\exp\left(\frac{-\Delta E_f^{\mathrm{As}I_{\mathrm{trans}}}(\boldsymbol{\epsilon})}{kT}\right) + f_V(0)\exp\left(\frac{-\Delta E_f^{\mathrm{As}V_{\mathrm{trans}}}(\boldsymbol{\epsilon})}{kT}\right)}. \quad (3)$$

In our calculation, 0.4 was used as a value of $f_I(0)$.[21] The change in energy due to strain is

$$\Delta E_f^{\mathrm{As}I,\mathrm{As}V_{\mathrm{trans}}}(\boldsymbol{\epsilon}) = -\Omega_0(\Delta\boldsymbol{\epsilon}^{\mathrm{As}I,\mathrm{As}V_{\mathrm{trans}}} - \Delta\boldsymbol{\epsilon}^{\mathrm{As}})\cdot\mathbf{C}^{\mathrm{Si}}\cdot\boldsymbol{\epsilon} + \frac{\Omega_0}{2}\boldsymbol{\epsilon}\cdot(\Delta\mathbf{C}^{\mathrm{As}I,\mathrm{As}V_{\mathrm{trans}}} \mp \mathbf{C}^{\mathrm{Si}})\cdot\boldsymbol{\epsilon}, \quad (4)$$

where Ω_0 is volume per lattice site, $\Delta\boldsymbol{\epsilon}$ is the induced strain vector, $\mathbf{C}$ is elasticity tensor, $\boldsymbol{\epsilon}$ is the applied strain vector, and $\mp$ corresponds to interstitial and vacancy. The second order term is much smaller than the first term for small strain and is neglected.

TABLE III. Binding energies for various As*V* configurations, calculated with equilibrium lattice parameter for GGA Si.

	As*V* 1NN	As*V* 2NN	As*V* 3NN
E_b (eV)	−1.22	−0.51	−0.43

TABLE IV. Induced strains of transition states and substitutional As. Strains are reported in reference to the GGA Si equilibrium lattice parameter.

Structure	AsI_{trans}	AsV_{trans}	As
$\Delta\epsilon$	0.309	−0.382	0.0186

Among many possible interstitial configurations, we find the ⟨110⟩ split interstitial to have the lowest formation energy, with the hexagonal interstitial as the transition state (see Fig. 6). Table II lists the formation energies of various As interstitials. Because the interstitial configuration we used to find migration path is shared by two hexagonal rings, As can continuously migrate from one ring to another without additional barrier after passing the transition state. Therefore the energy difference between ⟨110⟩ split and hex determines the migration barrier. The induced strain of the interstitial As transition state is isotropic due to the symmetry of hex site, and the hydrostatic strain calculation is sufficient to obtain the induced strain. The vacancy transition state is located between 2NN (2nd nearest neighbor) and 3NN.[22] Table III shows binding energies of As*V* at 1NN, 2NN and 3NN sites. We find that the As*V* transition state is equivalent to vacancy transition state in self-diffusion, and can be treated as isotropic.

Table IV shows induced strains of transition states. Energy versus hydrostatic strain for As complexes are shown in Fig. 7. The resulting changes in diffusivity due to I and V mechanisms are shown in Fig. 8. As expected and reported previously,[23] f_I increases under tensile strain and decreases under compressive strain (Fig. 9). As seen in Table IV, the magnitude of induced strain of vacancy transition state is larger than that of interstitial transition state. The larger fractional coefficient of vacancy diffusion at zero strain and

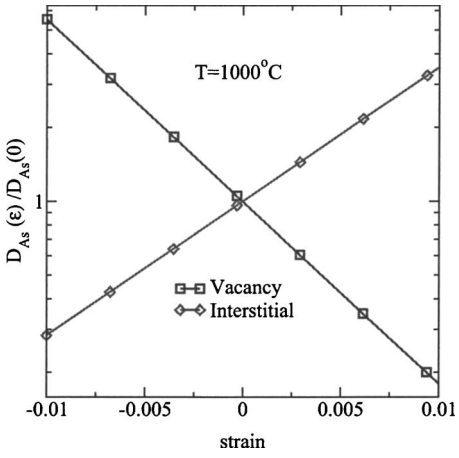

FIG. 8. Strain dependence of As diffusivity. Vacancy mechanism shows slightly stronger strain dependence than interstitial due to larger induced strain.

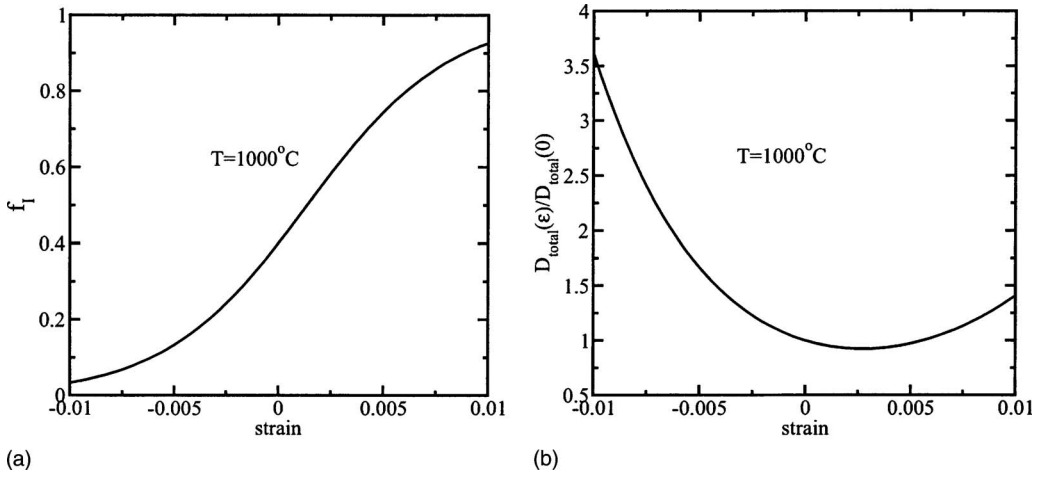

FIG. 9. Strain dependence of (a) fractional contribution to As diffusion by interstitial mechanism (f_I) and (b) total As diffusivity normalized to unstrained value. Diffusion mechanism changes from vacancy mediated to interstitial mediated in going from compressive to tensile strain.

stronger stress effect for vacancy mechanism result in total diffusivity enhancement under compressive strain and littlechange under tensile strain, consistent with experimental observations.[24]

IV. TRANSIENT ENHANCED DIFFUSION

The combined effect of stress on point-defect diffusion and B diffusion control transient enhanced diffusion (TED) of boron. We have developed a simple model to estimate the effect of stress on boron TED. Since calculations indicate that both I and B have anisotropic diffusion in the presence of anisotropic stress, it is of major interest to see how this translates into TED effects.

High dose implants lead to a supersaturation of interstitials during the early stages of dopant anneals. Since B diffuses dominantly via an interstitial mechanism (formation of a mobile BI pair), B equilibrium diffusivity D_B^* gets enhanced by orders of magnitude in the presence of I supersaturation. The B diffusivity is enhanced until C_I reaches C_I^* again. This one to one correspondence between I supersaturation and enhanced B diffusivity can be expressed in terms of[25]

$$\int \frac{D_B(t) - D_B^*}{D_B^*} dt \approx \int \frac{C_I(t) - C_I^*}{C_I^*} dt \approx \frac{R_p Q}{D_I C_I^*}, \tag{5}$$

where R_p is the projected range of the implant and Q is the dose of interstitials due to the implant (assuming a +1 model this is equivalent to the boron dose). D_I and C_I^* are the equilibrium I diffusivity and I concentration, respectively. The left hand side of Eq. (5) is directly related to $(Dt)_{TED}$, which is often used as a measure of TED, $(Dt)_{TED} = \int (D_B(t) - D_B^*) dt$. Combining these relations leads to

$$(Dt)_{TED} = R_p Q \frac{D_B^*}{D_I C_I^*}. \tag{6}$$

Since we determined the stress effects of D_B^* and $D_I C_I^*$, we now can also determine the relative change of TED in the presence of stress using Eq. (6). The ratio of $D_B^*/D_I C_I^*$ determines the stress effect on TED. In the case of biaxial strain, there are both in-plane (lateral) and out-of-plane (vertical) diffusion directions. In both cases, we assume that the total

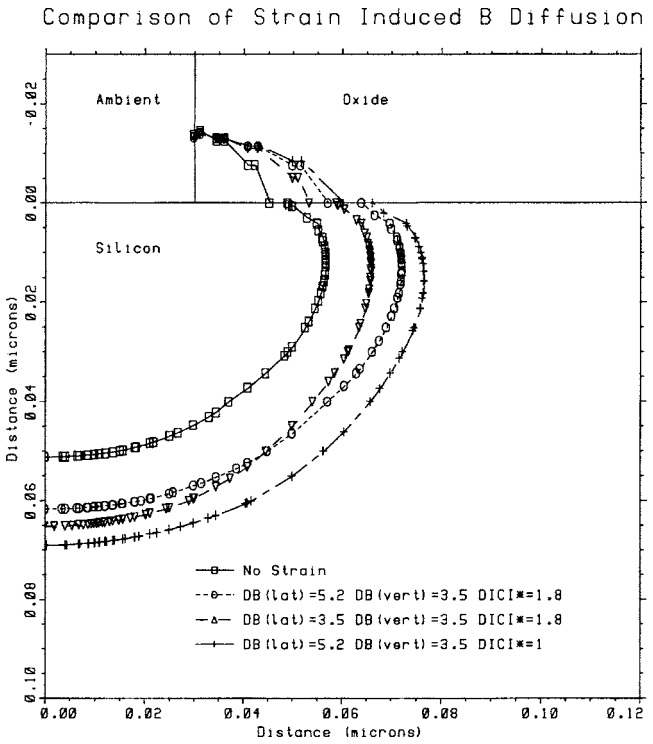

FIG. 10. Two-dimensional doping profiles showing effect of biaxial strain on B diffusion and TED near junction edge based on tensor (diagonal) diffusivity model implemented in TSUPREM4. The 4 curves (listed in order of vertical junction depth) are for: no strain effects (□), full anisotropic strain model (○), no anisotropy ($D_B^{lat} = D_B^{vert}$) (∇), and strain effect for just B, but not I (+). Under these conditions, the predicted lateral B diffusivity enhancement is larger (5.2) than the enhancement in vertical diffusivity (3.5). The enhancement in vertical I diffusion capacity (1.8) reduces the B diffusion enhancement due to TED in comparison to equilibrium conditions.

TED time is determined by the vertical diffusion of interstitials to the surface

$$\frac{(Dt)_{\mathrm{TED}}^{\mathrm{lateral}}(\epsilon)}{(Dt)^{\mathrm{TED}(0)}} = \left(\frac{D_{\mathrm{B}}^{*}(\epsilon)_{\mathrm{lateral}}}{D_I C_I^{*}(\epsilon)_{\mathrm{vertical}}}\right) \Bigg/ \left(\frac{D_{\mathrm{B}}^{*}(0)_{\mathrm{lateral}}}{D_I C_I^{*}(0)_{\mathrm{vertical}}}\right)$$

$$\frac{(Dt)_{\mathrm{TED}}^{\mathrm{vertical}}(\epsilon)}{(Dt)^{\mathrm{TED}(0)}} = \left(\frac{D_{\mathrm{B}}^{*}(\epsilon)_{\mathrm{vertical}}}{D_I C_I^{*}(\epsilon)_{\mathrm{vertical}}}\right) \Bigg/ \left(\frac{D_{\mathrm{B}}^{*}(0)_{\mathrm{vertical}}}{D_I C_I^{*}(0)_{\mathrm{vertical}}}\right). \quad (7)$$

In the case of 1% biaxial strain at 1000 °C, the results for the individual components are determined using the relations in this article and Ref. 6. Combining the results leads to an enhancement of lateral TED by a factor of 3.39, whereas vertical TED is predicted to be enhanced by a factor of 2.15.

The anisotropic diffusion of B predicted by DFT calculations has been implemented into TSUPREM4 which allows the specification of a diagonal diffusion tensor for dopants. The results of an example simulation are shown in Fig. 10. Note that the anisotropic diffusion leads to substantially greater broadening in lateral direction than would be predicted based on vertical enhancement, which is what is typically measured. Also, the enhancement of $D_I C_I^{*}$ under tensile stress reduces the diffusion enhancement under tensile stress for TED conditions compared to equilibrium.

V. CONCLUSIONS

In conclusion, we used *ab initio* (DFT) calculations to investigate the effect of stress on B and As diffusivities. B diffusion is enhanced under tensile and reduced for compressive strain. As diffusion is enhanced by compressive strain, but nearly unchanged for tensile strain. The calculations showed a strong anisotropy in the case of B diffusion under biaxial strain, with significant implications for controlling channel length and lateral abruptness. The enhancement for in-plane (lateral) diffusion is larger than for out-of-plane (vertical) diffusion. The full knowledge of the diffusion tensors enables the implementation of local stress effects in two-dimensional and three-dimensional TCAD process simulators.

ACKNOWLEDGMENTS

This work was supported by the Semiconductor Research Corporation. Most of the calculations were conducted using a computing cluster donated by Intel.

[1] J. L. Hoyt, H. M. Nayfeh, S. Eguchi, I. Aberg, G. Xia, T. Drake, E. A. Fitzgerald, and D. A. Antoniadis, in *IEDM '02. Digest. International Electron Devices Meeting*, 8–11 Dec. 2002 (IEEE, Piscataway, NJ, 2002), p. 23.
[2] K. Rim, J. L. Hoyt, and J. F. Gibbons, IEEE Trans. Electron Devices **47**, 1406 (2000).
[3] J. Welser, J. L. Hoyt, and J. F. Gibbons, IEEE Electron Device Lett. **15**, 100 (1994).
[4] W. Windl, M. Laudon, N. N. Carlson, and M. S. Daw, IEEE Comput. Sci. Eng. **3**, 92 (2001).
[5] M. J. Aziz, Appl. Phys. Lett. **70**, 2810 (1997).
[6] M. Diebel, Ph.D. thesis, University of Washington, Seattle, WA (2004).
[7] G. Kresse and J. Hafner, Phys. Rev. B **47**, 558 (1993).
[8] G. Kresse and J. Furthmüller, Phys. Rev. B **54**, 11169 (1996).
[9] D. Vanderbilt, Phys. Rev. B **41**, 7892 (1990).
[10] H. J. Monkhorst and J. D. Pack, Phys. Rev. B **13**, 5188 (1976).
[11] G. Mills, H. Jónsson, and G. K. Schenter, Surf. Sci. **324**, 305 (1995).
[12] H. Jónsson, G. Mills, and K. W. Jacobsen, *Classical and Quantum Dynamics in Condensed Phase Simulations* (World Scientific, Singapore, 1998), p. 385.
[13] G. Henkelman and H. Jónsson, J. Chem. Phys. **113**, 9978 (2000).
[14] G. Henkelman, B. P. Uberuaga, and H. Jónsson, J. Chem. Phys. **113**, 9901 (2000).
[15] W. Windl, M. M. Bunea, R. Stumpf, S. T. Dunham, and M. P. Masquelier, Phys. Rev. Lett. **83**, 4345 (1999).
[16] P. Kuo, J. L. Hoyt, J. F. Gibbons, J. E. Turner, and D. Lefforge, Appl. Phys. Lett. **66**, 580 (1995).
[17] Y. Zhao, M. J. Aziz, H.-J. Gossmann, S. Mitha, and D. Schiferl, Appl. Phys. Lett. **74**, 31 (1999).
[18] M. J. Aziz, Mater. Sci. Semicond. Process. **4**, 397 (2001).
[19] N. R. Zangenberg, J. Fage-Pedersen, J. Lundsgaard Hansen, and A. Nylandsted Larsen, J. Appl. Phys. **94**, 3883 (2003).
[20] A. Ural, P. Griffin, and J. Plummer, J. Appl. Phys. **85**, 6440 (1999).
[21] J. D. Plummer, M. D. Deal, and P. B. Griffin, *Silicon VLSI Technology: Fundamentals, Practice, and Modeling* (Prentice–Hall, Upper Saddle River, NJ, 2000).
[22] J. Xie and S. Chen, J. Phys. D **32**, 1252 (1999).
[23] O. Sugino and A. Oshiyama, Phys. Rev. B **46**, 12335 (1992).
[24] N. Sugii, J. Appl. Phys. **96**, 261 (2004).
[25] H. Meyer and S. T. Dunham, in *Mater. Res. Soc. Symp. Proc.* (MRS, Warrendale, PA, 2002), Vol. 717, p. C4.8.1.
[26] M. R. Sardela, H. H. Radamson, J. O. Ekberg, J.-E. Sundgren, and G. V. Hansson, Semicond. Sci. Technol. **9**, 1272 (1994).